N89-10851

Summary of an Experimental Investigation

On the Ground Vortex

Michael L. Billet
John M. Cimbala

The Pennsylvania State University
Applied Research Laboratory
Post Office Box 30
State College, PA 16804

Introduction

The impingement of a circular jet exhaust flow on a ground plane results in the formation of a wall jet which flows radially from the point of impingement along the ground surface. Forward motion of the jet source or the introduction of a cross-flowing freestream interacts with the wall jet to create a stagnation line and tends to roll the wall jet back on itself forming a horseshoe-shaped ground vortex, as illustrated in Figure 1. Generally taking the shape of an ellipse whose major axis is aligned with the freestream flow, the location of this stagnation line is dependent on the ratio of the freestream and wall jet dynamic pressures, the distance from the jet to the ground plane, and the injection angle of the exhaust into the freestream flow. The location of the center of the vortex is downstream from this stagnation line and at a height above the ground which is also a function of the jet-to-cross-flow velocity ratio. When flow conditions are appropriate for its formation, this vortex is a major source of induced flow in the near field. Shown in Figure 2, is a side view diagram of the ground vortex and the coordinate system used.

The results of an experimental investigation into the position and characteristics of the ground vortex are summarized in this paper. The ARL/PSU 48-inch wind tunnel was modified to create a testing environment suitable for the ground vortex study. Flow visualization was used to document the jet-crossflow interaction and a two-component Laser Doppler Velocimeter (LDV) was used to survey the flowfield in detail. Measurements of the ground vortex characteristics and location as a function of freestream-to-jet velocity ratio, jet height, pressure gradient and upstream boundary layer thickness were obtained.

Test Facility

A 3.0 inch diameter open-jet facility was fabricated and inserted through one side of the test section of the 48-inch wind tunnel as shown in Figure 3. Details of the wind tunnel can be found in Reference 1. The jet features a 16:1 contraction ratio and is equipped with two wire mesh screens and honeycomb to improve the flow quality. The 150.0 ft/sec jet was powered by a variable speed 5.0 hp blower which injected air from the wind tunnel at a port far downstream from the test chamber.

The test section of the wind tunnel can be separated which permitted the horizontal jet to exhaust into the still air in the absence of any physical constraint. Velocity surveys to measure jet characteristics were conducted at 1.0, 2.0, 3.0, 4.0 and 6.0 jet diameters with V_j = 150 ft/sec. The axisymmetric jet mean velocity profiles obtained with a five-hole probe are shown in Figure 4 for the vertical plane. In addition turbulence measurements were made using a hot-wire anemometer at an axial distance of 2.0 jet diameters. The turbulence intensity at the centerline was experimentally measured to be approximately 2%.

The test chamber was formed by two 8.03 ft long wooden panels with circular arc leading edges. The jet tube extended 6.00 in. through the center of the 0.75 in. thick, 37.00 in. wide jet plane at a streamwise distance 47.0 in. downstream of its leading edge. The jet plane was at a fixed streamwise location, but could be rotated to a positive or negative angle of attack. The movable 43.0 in. wide ground plane was designed to facilitate conducting various phases of the test program. The ground plane was attached to inserts along the tunnel walls, and could be positioned at 1, 2, 3, 4 or 6 jet diameters from the jet exit plane. The ground board was also equipped with interchangeable 2.0 ft by 3.0 ft window inserts. Three windows were available for various phases of the test program, i.e., a glass flow visualization window instrumented with fluorescent mini-tufts, a glass window for LDV surveys, and a plexiglass window instrumented with static pressure taps. The leading edge of the window insert was 18.75 in. upstream of the jet centerline.

Because the wind tunnel facility is symmetric, it was possible to rotate the entire installation of Figure 3 by 90°. Both orientations (ground plane vertical and ground plane horizontal) were used in this experimental program. The vertical-ground-plane orientation was used for the preliminary measurements and surface flow visualizations, while the horizontal-ground-plane orientation was more convenient for the smoke-wire flow visualizations and detailed LDV measurements.

Wall-to-wall surveys of the velocity field between the ground plane and the jet plane were conducted with a five-hole probe to document the uniformity of the test chamber with the jet off. Figure 5 shows a typical survey at h/D_j = 2.0, and at V_∞ = 60.0 ft/s. The boundary layers on both walls can be seen from the streamwise velocity component, which is quite uniform in the core flow between the walls; the other two velocity components are negligibly small.

In addition velocity profiles of the wall jet itself were obtained with the jet on and the wind tunnel turned off. Figure 6 shows a survey obtained with the total-head boundary layer probe for V_j = 150ft/sec, h/D_j = 3.0 and the probe located 5.33 jet diameters upstream of the jet centerline. Also shown in this

figure is the theoretical wall jet profile, calculated from the semi-empirical relations found in Reference 2. The agreement between experiment and theory is excellent.

Since the entire test chamber lies within the confines of a wind tunnel test section, it is likely that when the jet is then turned on, the flow field around the jet and ground planes would be altered. This effect was studied both with flow visualization and surface static pressure measurements. These results are discussed in detail in Reference 3.

Based on these results, the following procedure was employed to establish zero pressure gradient, constant cross flow velocity between the plates upstream of the region of interest: 1). The reference cross-flow velocity was measured with a pitot-static tube located far enough upstream, between the jet and ground planes, and outside of any side wall boundary layers so as to be well within the region of zero pressure gradient (i.e. upstream of any jet effects). The probe location $x/D_j = 9.67$ was found to satisfy these requirements for all test cases. 2). The wind tunnel velocity was adjusted with the jet on, so that an accurate V_∞ and p_∞ could be established and recorded. In this manner, the blockage effect of the jet was reduced.

Summary of Experimental Results

Flow Visualization

The window instrumented with the fluorescent mini-tufts was used to obtain a first-order measurement of the ground vortex location. These data were then used to facilitate the later phases of the measurements. Surface flow visualization studies were conducted at the four values of V_∞/V_j [V_∞ = 15, 30, 45, 60 ft/sec, V_j = 150 ft/sec] and the five h/D_j locations [h/D_j = 1.0, 2.0, 3.0, 4.0 and 6.0]. The primary data obtained were photographs of the resulting flow patterns and the location of the separation line and the maximum penetration line of the recirculation region on the ground board. The quantities x_s, x_i, and x_{mp} were measured from the centerline of the jet tube and were determined by both real time observation of the mini-tuft pattern and later analysis of the photographs.

The impingement point x_i was easily identified from the photographs as the point from which the tufts spread out radially. The separation line was determined from the photographs as the line where the mini-tufts change orientation from upstream to downstream. Separation point x_s is defined here as the distance upstream from the jet centerline to this separation line. The leading edge or maximum penetration line is defined as the location upstream of which the mini-tufts align themselves parallel to the cross flow. Maximum penetration point x_{mp} is defined as the streamwise distance from this line to the jet centerline.

A comparison between the location of the separation point defined from the photographs and obtained from plate pressure distribution data is shown in Figure 7. The accuracy of the photographic data is $\pm$ 0.25 jet diameters which corresponds to $\pm$ 1 mini-tuft spacing. A discussion of the pressure distribution data is given in a following section.

In addition to the surface flow visualizations, smoke-wire photographs provided instantaneous views of the ground vortex itself. Again, photographs were taken for the various combinations of h/D_j and V_∞/V_j. Figure 8 shown the smoke streakline pattern for $h/D_j = 2.0$. It is important to note that the jet tube protruded two jet diameters down from the jet plane, and therefore the total height between ground and jet planes was four jet diameters. It is clear that the ground vortex decreases in size and moves further downstream as the cross flow velocity increases. It appears that very little of the freestream fluid enters the ground vortex; the freestream apparently jumps over the vortex, much as it would over a solid body obstruction in the flow. As will be discussed below, velocity measurements have shown that the ground vortex is really not a vortex at all, but rather a region of separated recirculating flow. The "ground vortex" is thus more properly referred to as a separation bubble.

Note that photos a) and b) of Figure 8 were taken for identical test chamber conditions, but at different times (about a minute apart). Comparing the two, one can see the unsteadiness in the flow pattern. Both photos are instantaneous snap shots, and therefore have "frozen" the motion at one arbitrary point in time. The flow field captured in photo a) contains one large separation bubble, while that of photo b) appears to contain two separation bubbles.

Pressure Distributions

One of the interchangeable window inserts on the ground plate was instrumented with an array of 72 static pressure taps. The time-averaged static pressure distribution along the ground plane was measured for each combination of h/D_j and V_∞/V_j. The maximum resolution of a single pressure survey was limited to the distance between pressure taps in the array; however, the resolution was enhanced by shifting the ground plane by small amounts in the streamwise direction, with the jet location remaining fixed.

Figure 9 shows a typical smoothed static pressure distribution along the centerline of the ground plane for the case $h/D_j = 3.0$ and $V_\infty/V_j = 0.2$ The impingement point x_i of the jet is easily identified as the point of maximum C_p. Moving upstream (left to right in Figure 9) the pressure coefficient drops to a negative value, rises again above zero, and then slowly returns to zero far upstream. Colin and Olivari [2] have identified the negative C_p region as the approximate location of the ground vortex, with x_v the vortex center at the minimum C_p point. The zero-crossing point has been labeled x_s on Figure 9 and has been found to correspond to the separation point identified by the mini-tuft surface flow-visualization technique. Similar pressure distributions along the centerline of the ground plane have been taken for various values of h/D_j and V_∞/V_j. The zero-crossing point is compared in Figure 7 to the separation point determined from the mini-tuft photographs. The agreement is excellent except for the lowest velocity case ($V_\infty/v_j = 0.1$).

The static pressure tap array was also used to obtain pressure distributions along the ground plane at points away from the centerline. Seven streamwise rows of taps were instrumented, and labeled rows A-G with G being the centerline row. Each row was 1.5 in. (0.5 jet diameters) apart in the z-coordinate direction. A typical set of transverse pressure distributions is shown in Figure 10 for the

case h/D_j = 3.0 and V_∞/V_j = 0.2. The "horseshoe" shape of the separation bubble can be inferred from this figure; i.e. dip in the pressure distribution upstream of impingement shifts downstream and decreases in magnitude as one moves further and further away from the centerline.

Laser Doppler Velocimeter Measurements

A schematic of the instrumentation for the Laser Doppler Velocimetry tests is presented in Figure 11. A two-component LDV system was used to survey the region upstream of the jet perpendicular to the ground plane centerline. The system was positioned using a three-axis traversing mechanism.

A smoke generator shown in Figure 11, which burns 'Punk' incense sticks, was used to seed the flow. A sample of the smoke was collected in a millipore filter; the size of the smoke particles was under 1 μm as determined with a scanning electron microscope. The seeding smoke was introduced into the flow through four ports located along the centerline of the ground plane. Two ports were selected for introducing seeding material into the jet flow and two parts for seeding the freestream.

Histograms of the velocity distribution at each point were obtained and analyzed statistically. A representative vector plot showing mean data is given in Figure 12 for V_∞/V_j = 0.2, and h/D_j = 4.0. A sample histogram is shown in Figure 13 for a point near the center of the vortex.

As can be noted in Figure 13, the flow within the ground vortex is extremely unsteady; however, the vector plot provides a visualization of the mean flow. For all cases measured, the cross-section through the ground vortex has an elliptical shape. It can also be noted that the flow is separated upstream of the vortex. The jet flow along the plate decreases and eventually reaches zero upstream of the vortex.

Discussion

A comparison with experimental data is shown in Figure 14 with the predicted curve of Colin and Olivari [2] and the model of Abbott [4]. The best comparison is obtained with the model of Abbott [4]. Abbott [4] showed that his data collapsed universally to the simple expression that the wall jet penetrates upstream to a point where, under stationary conditions, the maximum velocity of the wall jet would be approximately twice that of the oncoming freestream.

Unsteadiness in the flow field was observed, particularly at the lower values of V_∞/V_j. As discussed above, two instantaneous snap shots of the separation bubble, taken at different times, can appear drastically different, even for identical configurations and velocities. A most striking example of this is shown in Figure 8, for h/D_j = 2.0 and V_∞/V_j = 0.1. A likely candidate for the source of this unsteadiness is the amplification of shear layer vortices shed from the lip of the jet. These shear layer vortices can be most clearly seen in photo a) of Figure 8. It appears that the vortices convect upstream along the wall, and then fold back around the separation bubble. As they convect back toward the jet, the vortices may be amplified to the point of sudden bursting, which disrupts the entire flowfield.

Conclusions

A test facility suitable for the study of the ground vortex resulting from a jet impinging on a ground plane in the presence of a cross flow has been developed. Tests have defined the aerodynamic characteristics of the test chamber, the ground plane static pressure distributions, and flow patterns associated with the ground vortex. A summary of findings is listed below, not all of which have been discussed here; further details can be found in Reference 3:

1) For a given jet-exit-to-ground-plane height h/D_j, the ground vortex moved downstream and decreased in size and strength as freestream-to-jet velocity ratio V_∞/V_j was increased.

2) The separation point x_s of the wall jet on the ground plane was measured with both fluorescent mini-tuft surface flow visualization and static pressure measurements on the ground plane; agreement between the two techniques is excellent. Namely, the separation point corresponds to the zero-crossing point of the static pressure distribution.

3) The addition of a large flat plate, flush-mounted to the jet exit plane, forced the ground vortex to move downstream significantly and to decrease in size.

4) Within the limited range of pressure gradients obtainable with the present experimental setup, only a small effect of streamwise pressure gradient was found. There was a tendency for the separation point to move upstream with increasing pressure gradient.

5) Artificial thickening of the oncoming boundary layer on the ground plane resulted in further upstream penetration of the wall jet, but the effect was not as great as anticipated. Differences in boundary layer thickness are therefore not sufficient to account for the large scatter in data from various experimenters. Further differences, such as the jet and ground plane motion need to be explored.

6) The present experimental data for separation point location do not agree with the theory or measurements of Colin and Olivari [2], but agree fairly well with the empirical relationship suggested by Abbott [4].

7) LDV surveys indicate that the ground vortex is elliptical in shape, and does not have a velocity field describable by a classical free vortex. The ground vortex is thus really not a vortex at all, but rather a recirculating separation bubble, driven by the opposing wall jet and freestream flows.

8) Unsteadiness was observed in the separation bubble, particularly at the smaller values of V_∞/V_j (~0.1). It is conjectured that these fluctuations may be related to large-scale coherent vortical structures shed from the lip of the jet. No attempt was made to quantify this phenomenon, but should be considered during future experimentation.

References

1. "Garfield Thomas Water Tunnel Test Facilities," Applied Research Laboratory, The Pennsylvania State University, January 1980.

2. Colin, P. E. and Olivari, D., "The Impingement of a Circular Jet Normal to a Flat Surface With and Without a Cross Flow," Von Karman Institute Final Technical Report, January 1969, United States Defense Technical Information Center Technical Report AD688953.

3. Cimbala, J. M., Stinebring, D. R., Treaster, A. L., and Billet, M. L., "Experimental Investigation of a Jet Impinging on a Ground Plane in the Presence of a Cross Flow," Naval Air Development Center, Contractors Report NADC-87019-60, March 1987.

4. Abbott, W. A., "Studies of Flow Fields Created by Vertical and Inclined Jet When Stationary or Moving Over a Horizontal Surface," RAE CP No. 911, 1967.

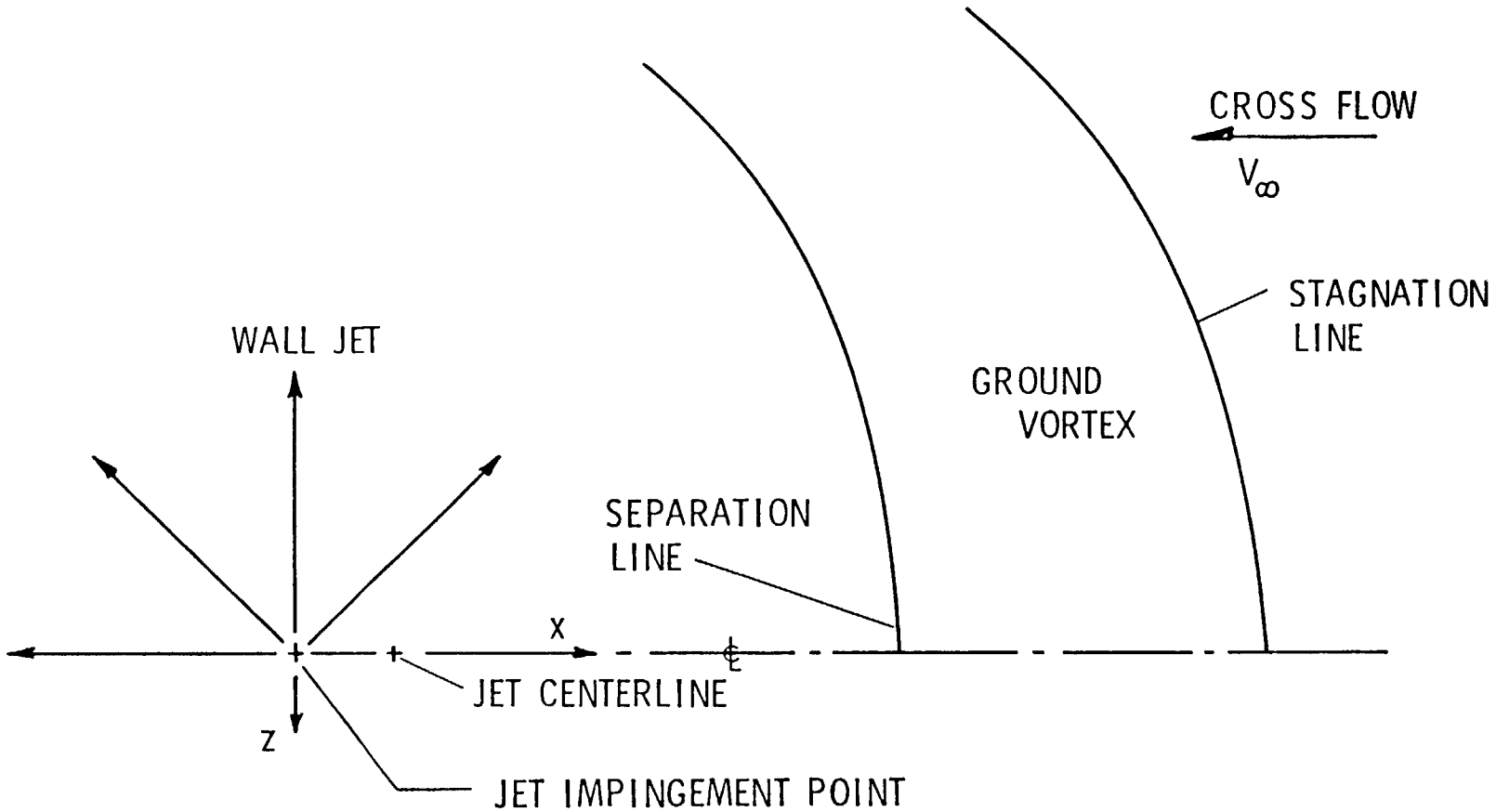

Figure 1. Horseshoe-Shaped Stagnation Line on Ground Plane (Plan View).

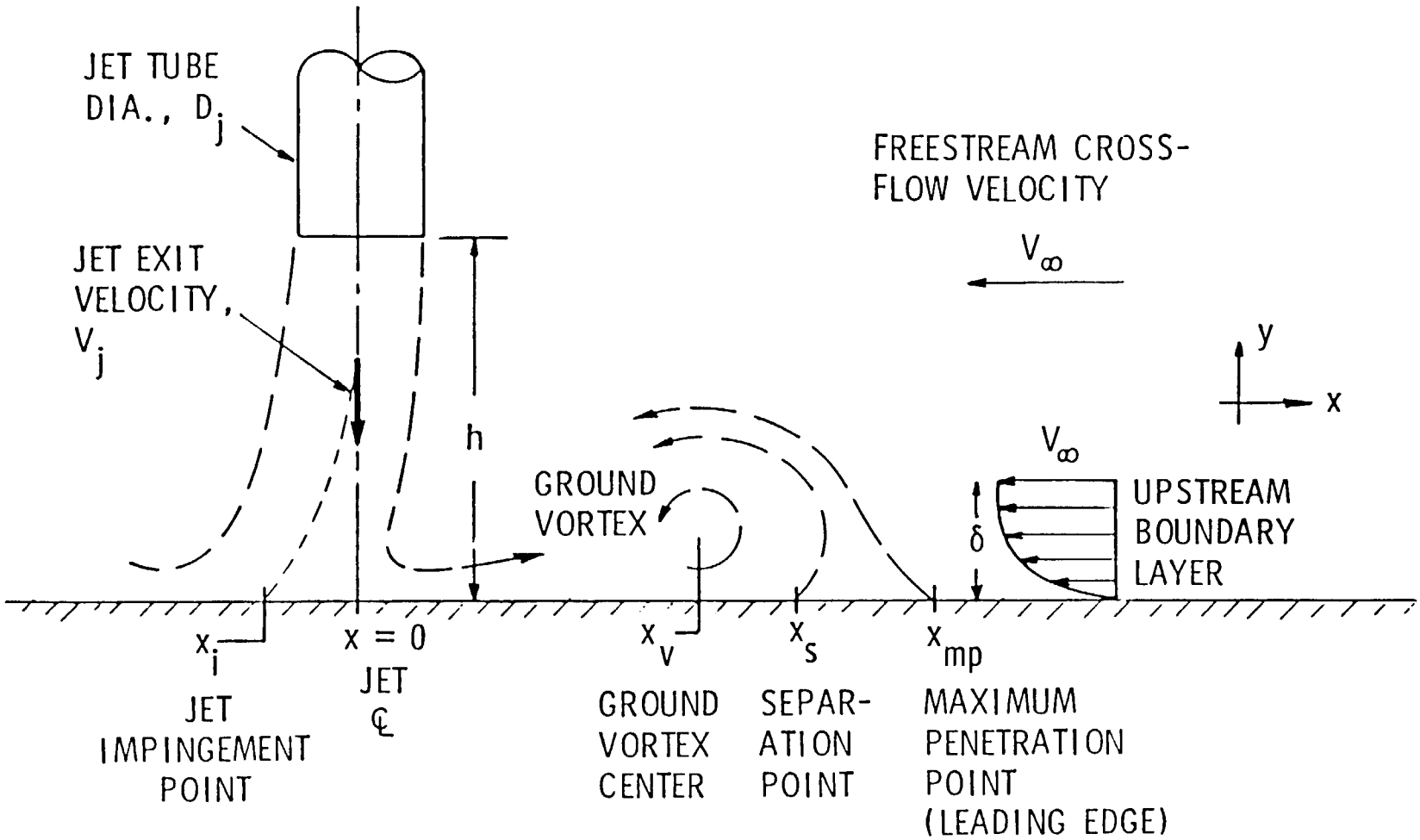

Figure 2. Ground Vortex Formed by a Jet Impinging Normally on a Flat Plate in a Cross Flow.

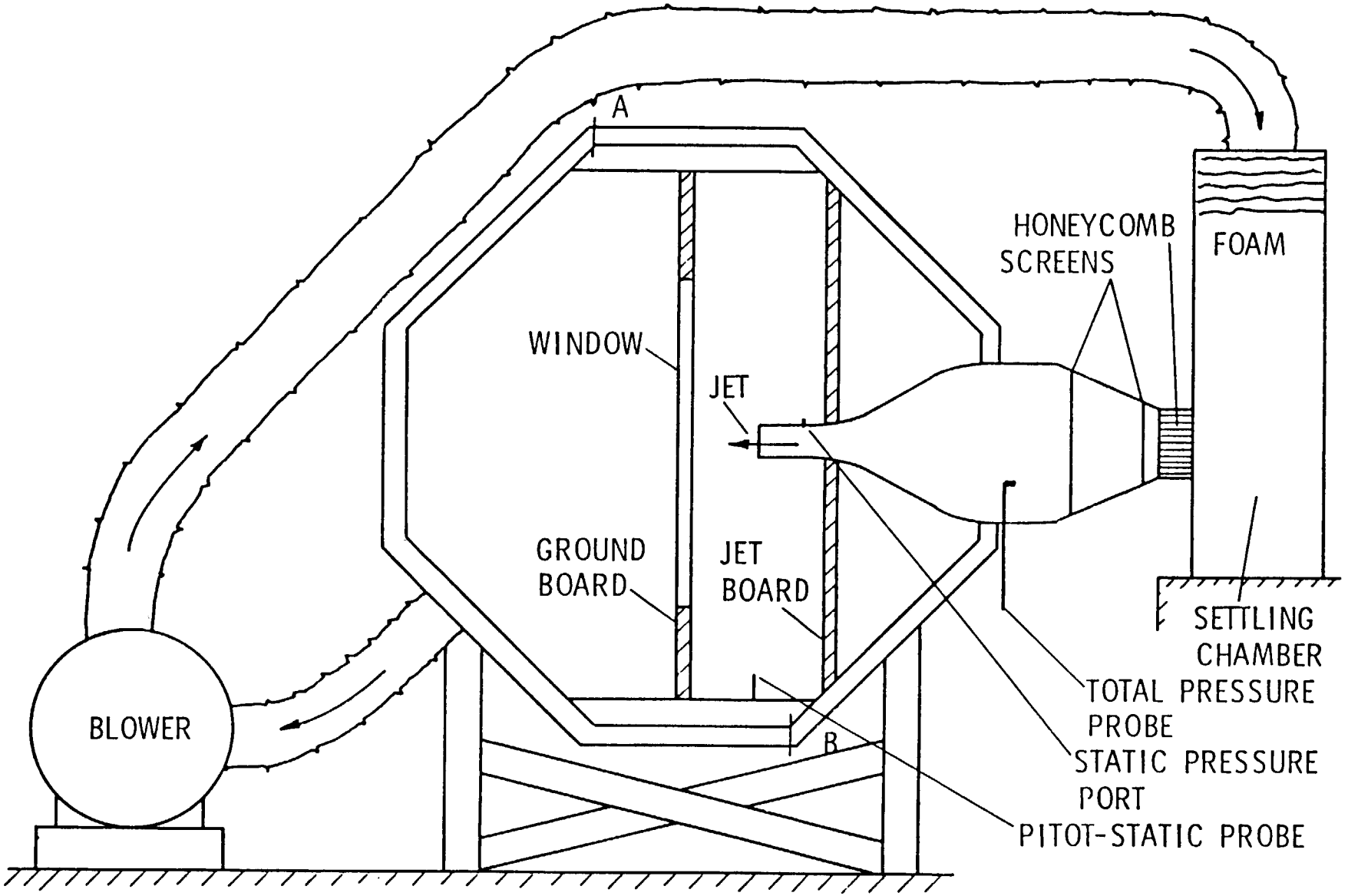

Figure 3. Jet Installation in Wind Tunnel (Vertical Ground Plane).

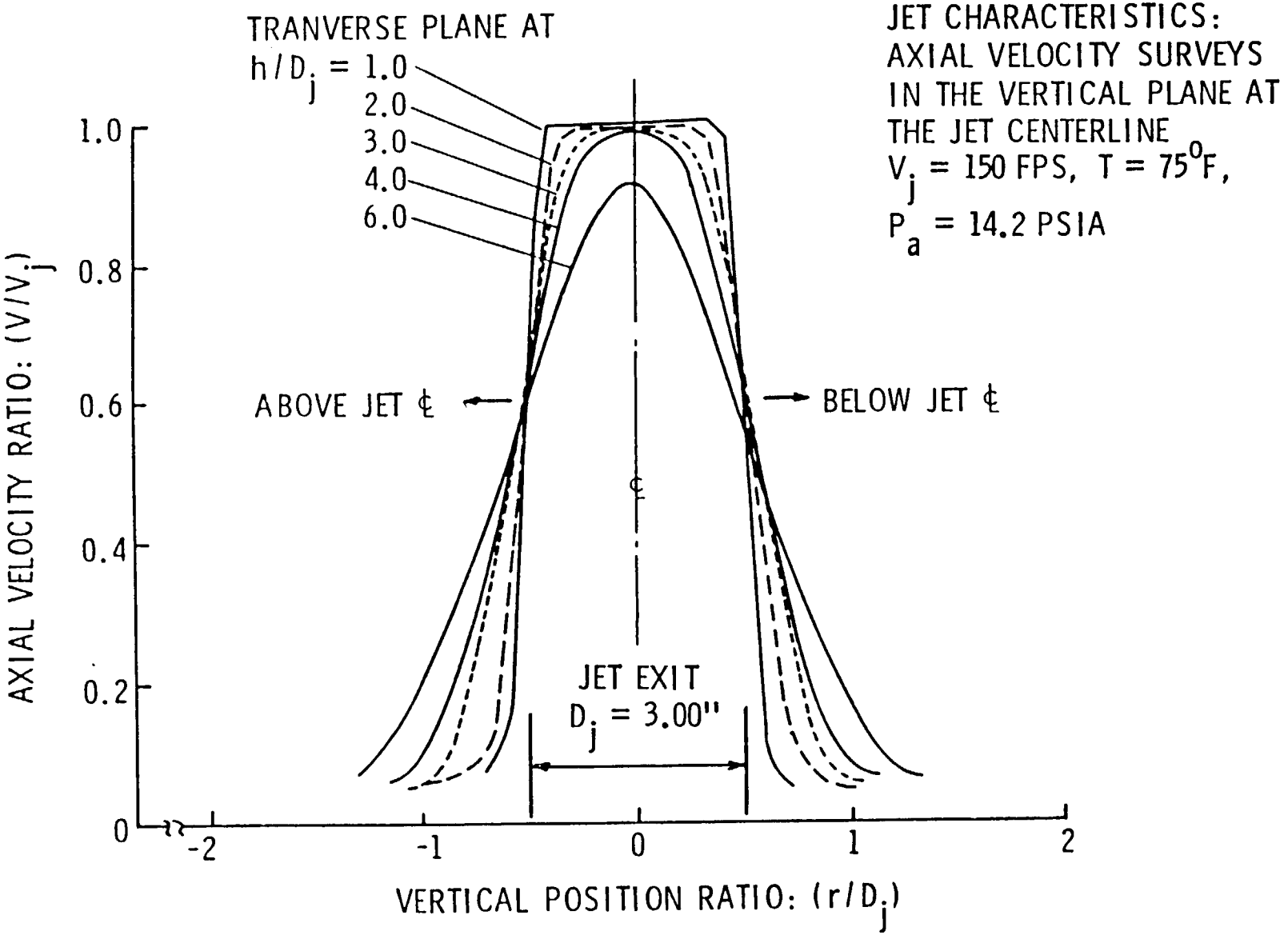

Figure 4. Jet Characteristics - Mean Velocity Surveys.

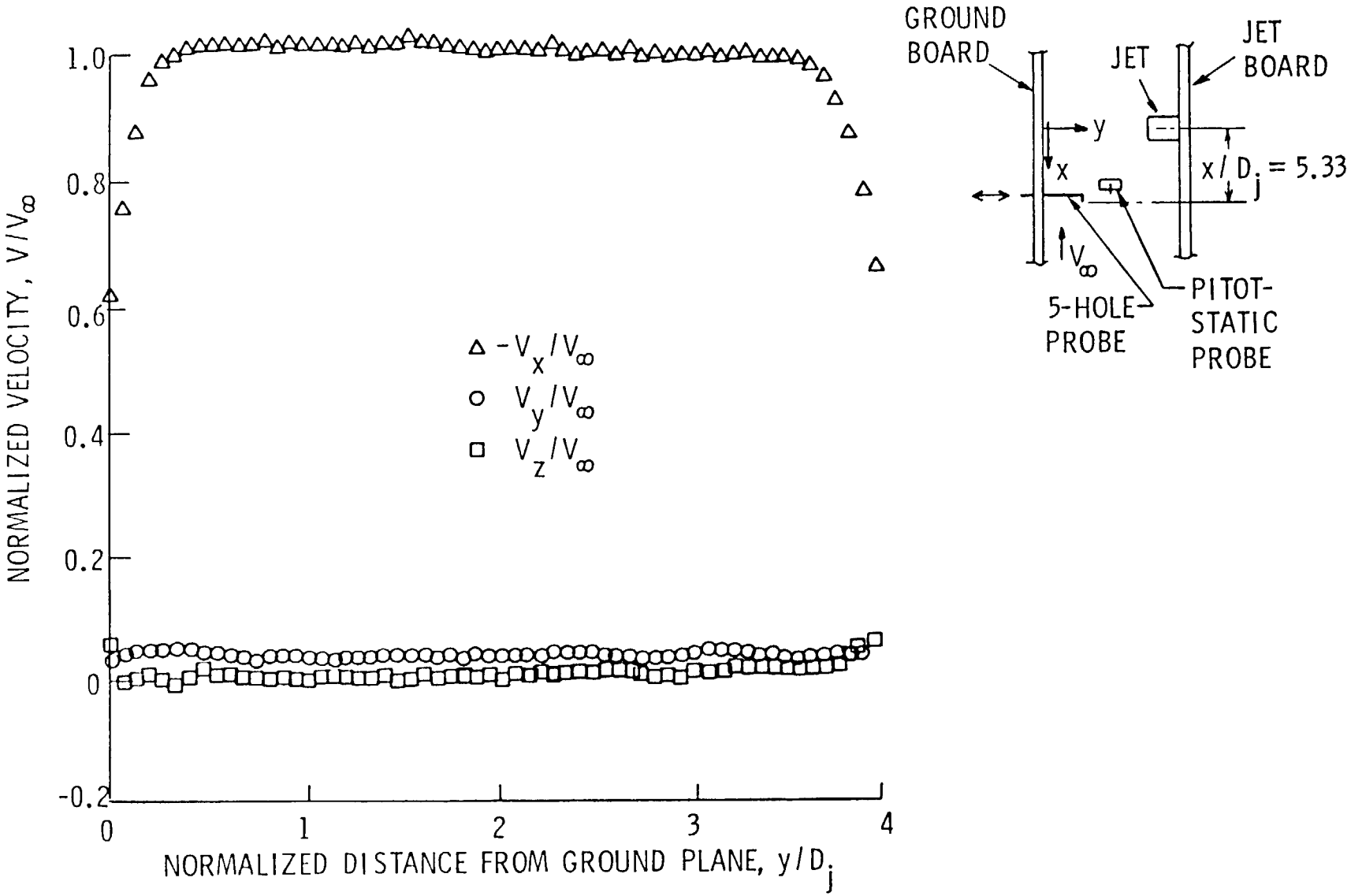

Figure 5. Test Chamber Velocity Survey at h/D_j = 2.0, and at V_∞ = 60.0 ft/s (18.3 m/s) with Jet Turned Off.

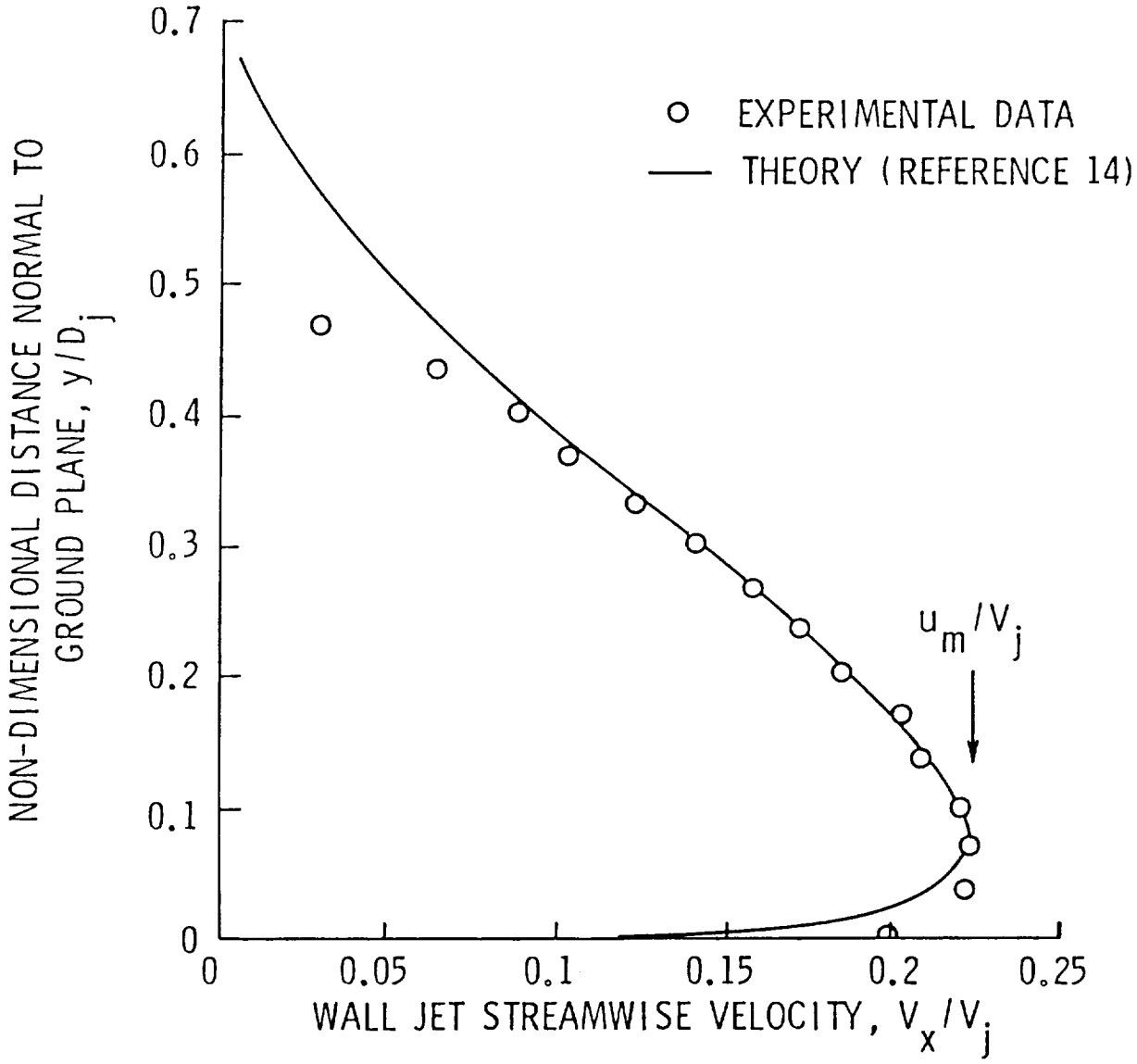

Figure 6. Wall Jet Velocity Profile at h/D_j = 3.0, x/D_j = 4.8, with Jet Velocity V_j = 150 ft/s (45.7 m/s), and No Cross Flow.

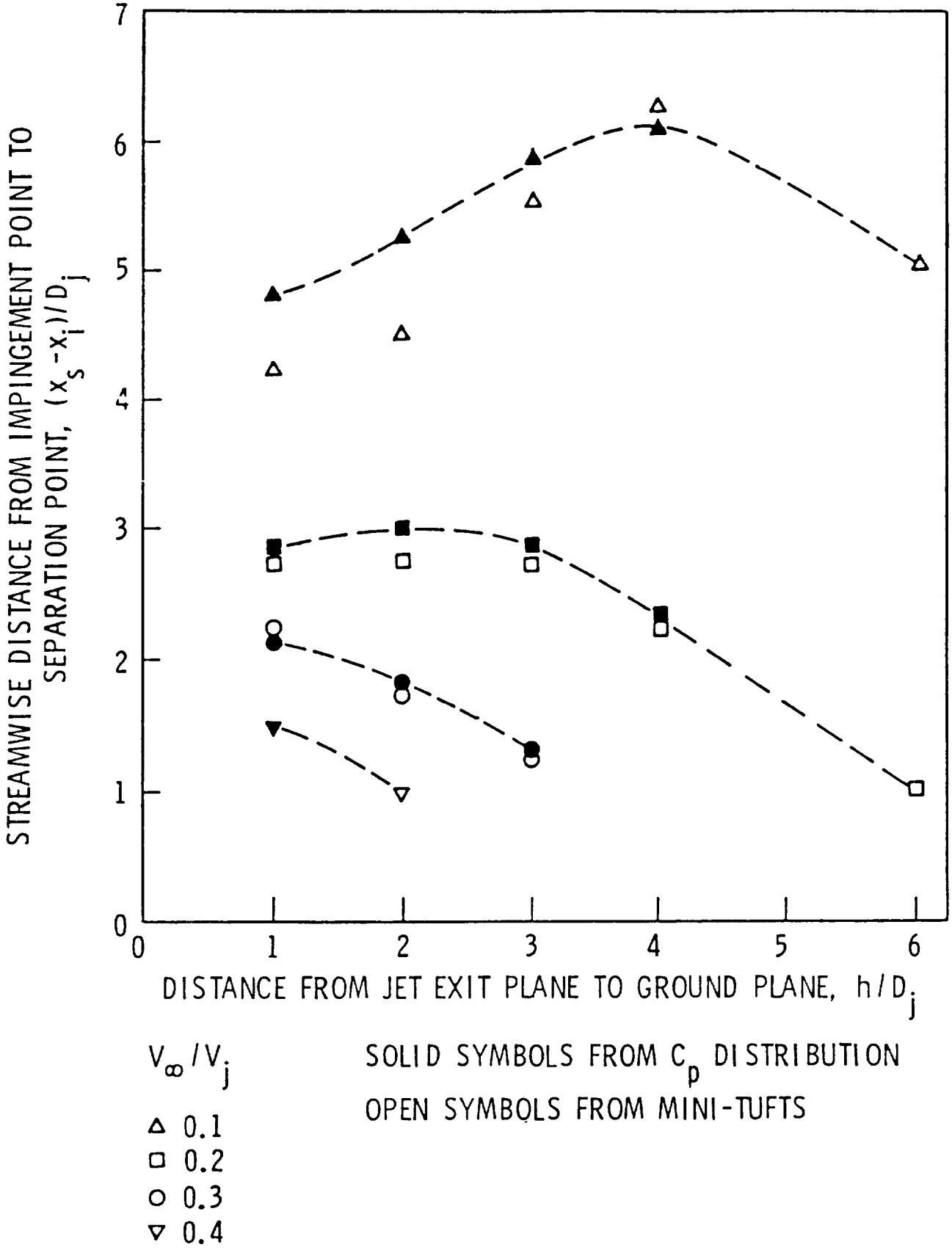

Figure 7. Measurement of Separation Point Location as a Function of Ground-Plane-to-Jet Distance for Four Velocity Ratios.

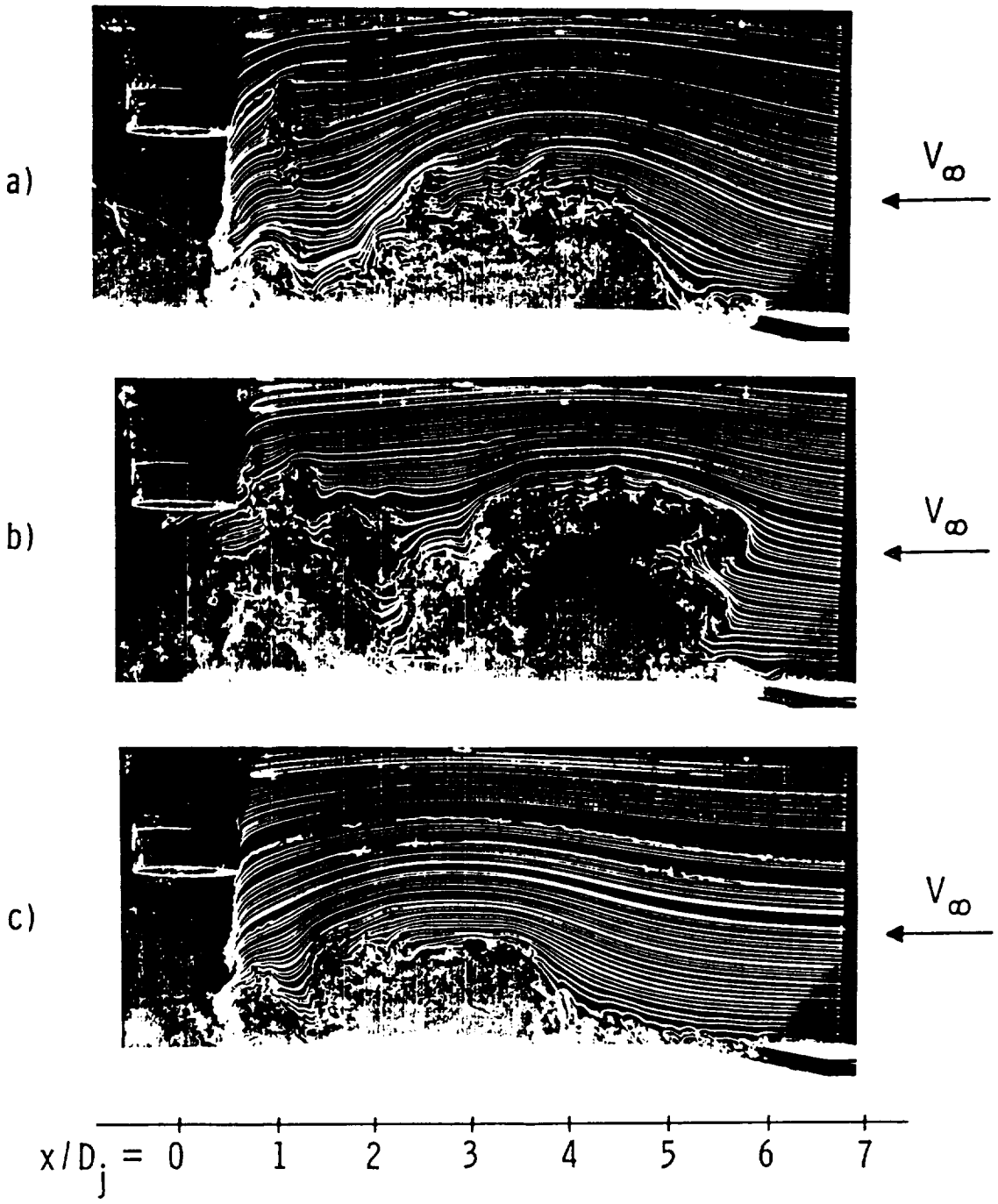

Figure 8 . Smoke-wire Photographs of Separation Bubble for h/D_j = 2.0, Standard Configuration, V_∞/V_j = a) 0.1, b) 0.1, c) 0.15, d) 2.0, e) 0.25, and f) 0.30. (Photos a) and b) are for identical conditions, but different times, and illustrate the unsteadiness.)

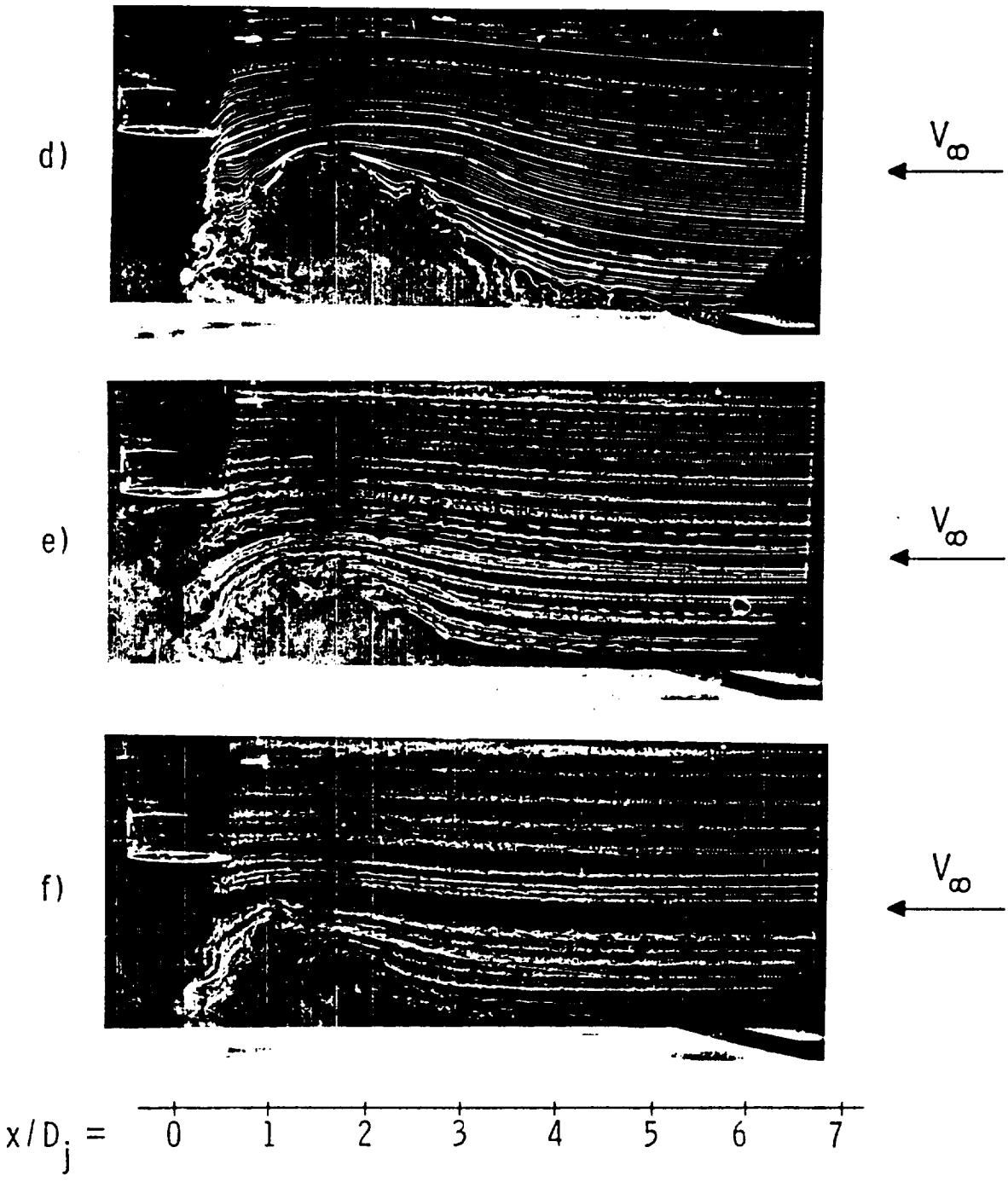

Figure 8. (Cont.)

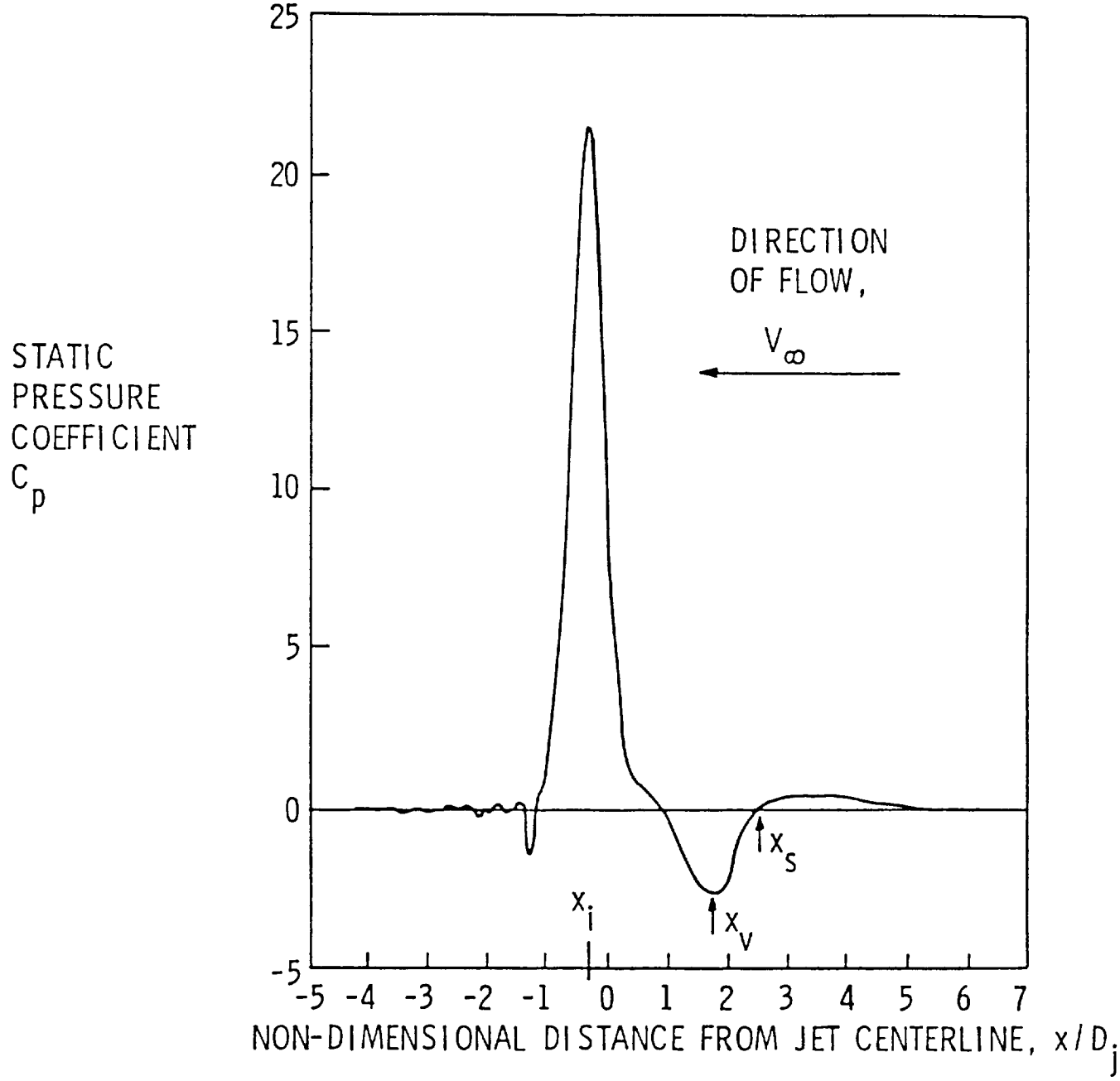

Figure 9. Static Pressure Coefficient Distribution Along Centerline of Ground Plane for $h/D_j = 3.0$, $V_\infty/V_j = 0.2$

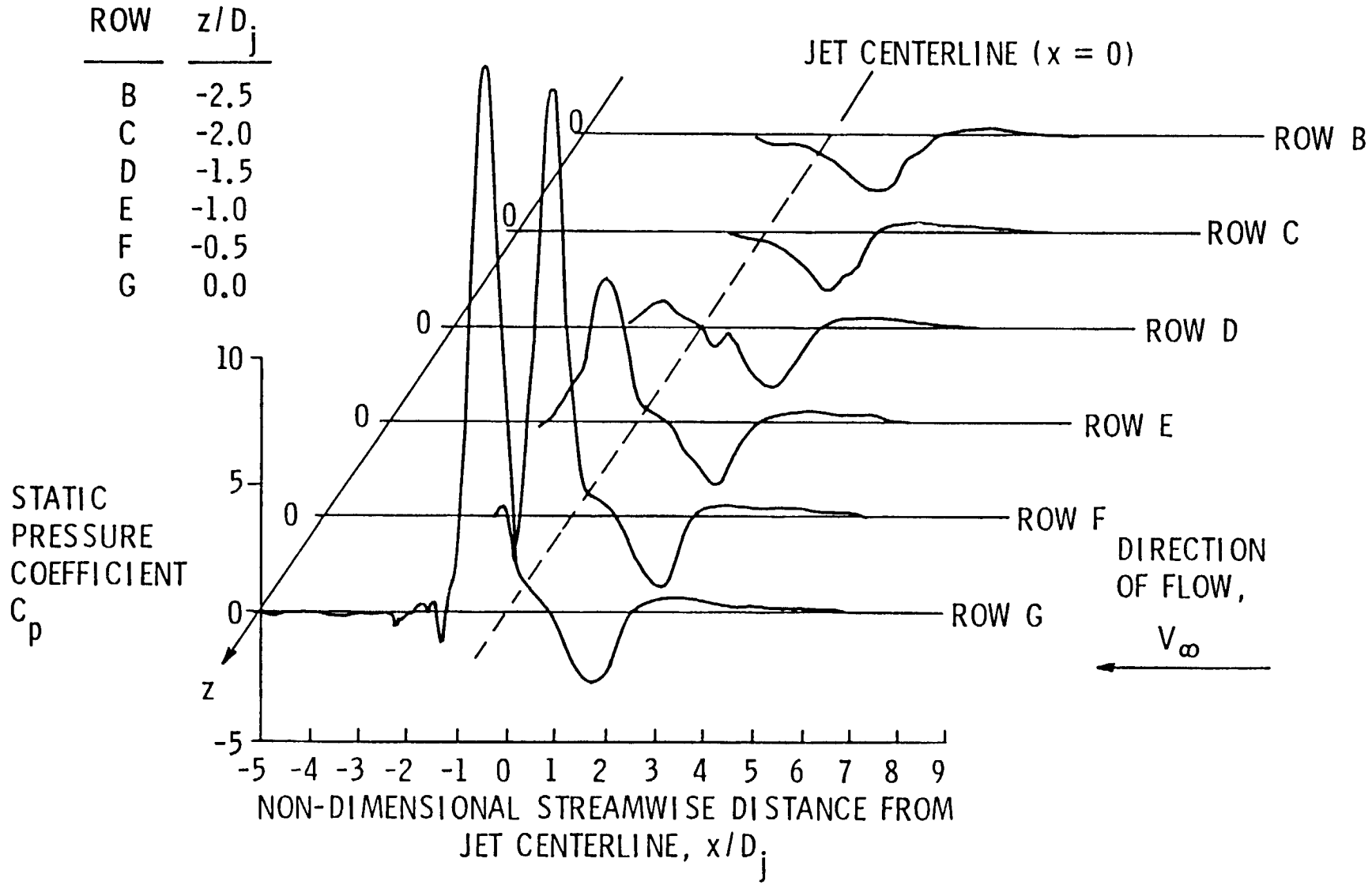

Figure 10. Static Pressure Distribution Along the Ground Plane as a Function of Streamwise and Transverse Distances from the Jet Centerline, $h/D_j = 3.0$, $V_\infty/V_j = 0.2$

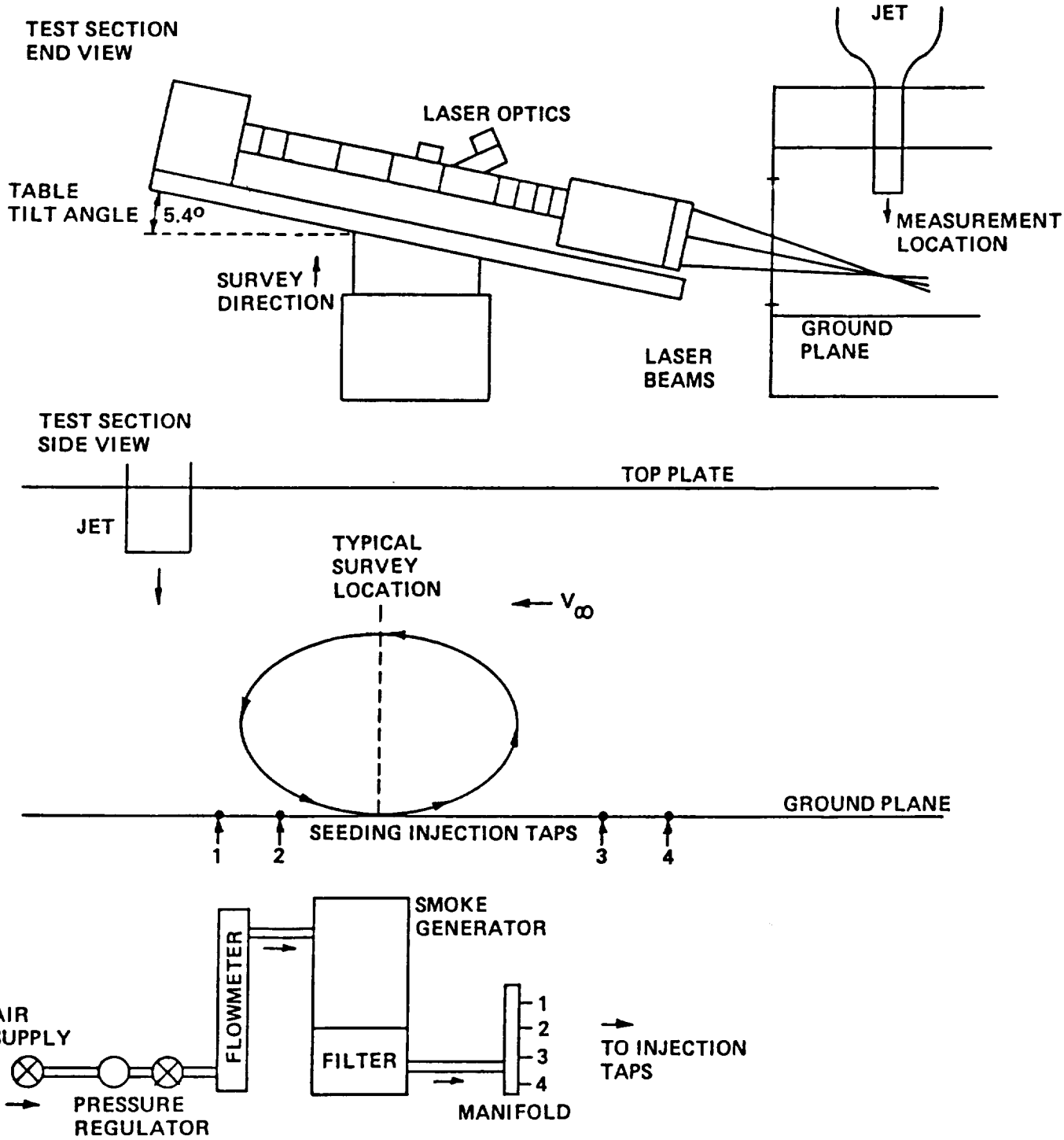

Figure 11. Schematic of Test Setup for LDV Surveys.

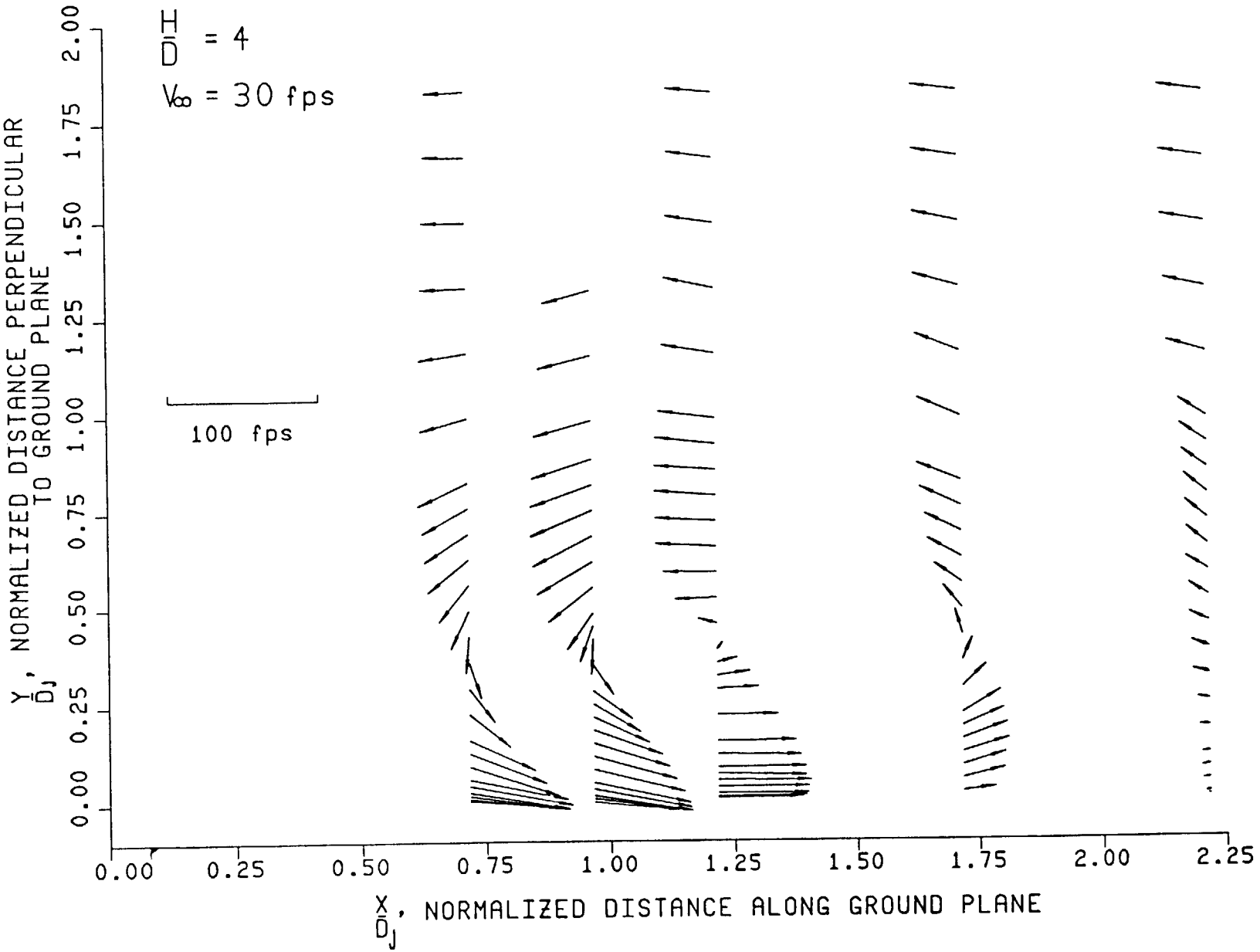

Figure 29. Vector Plot of Velocity Field for V_∞/V_j = 0.2 and h/D_j = 4.0

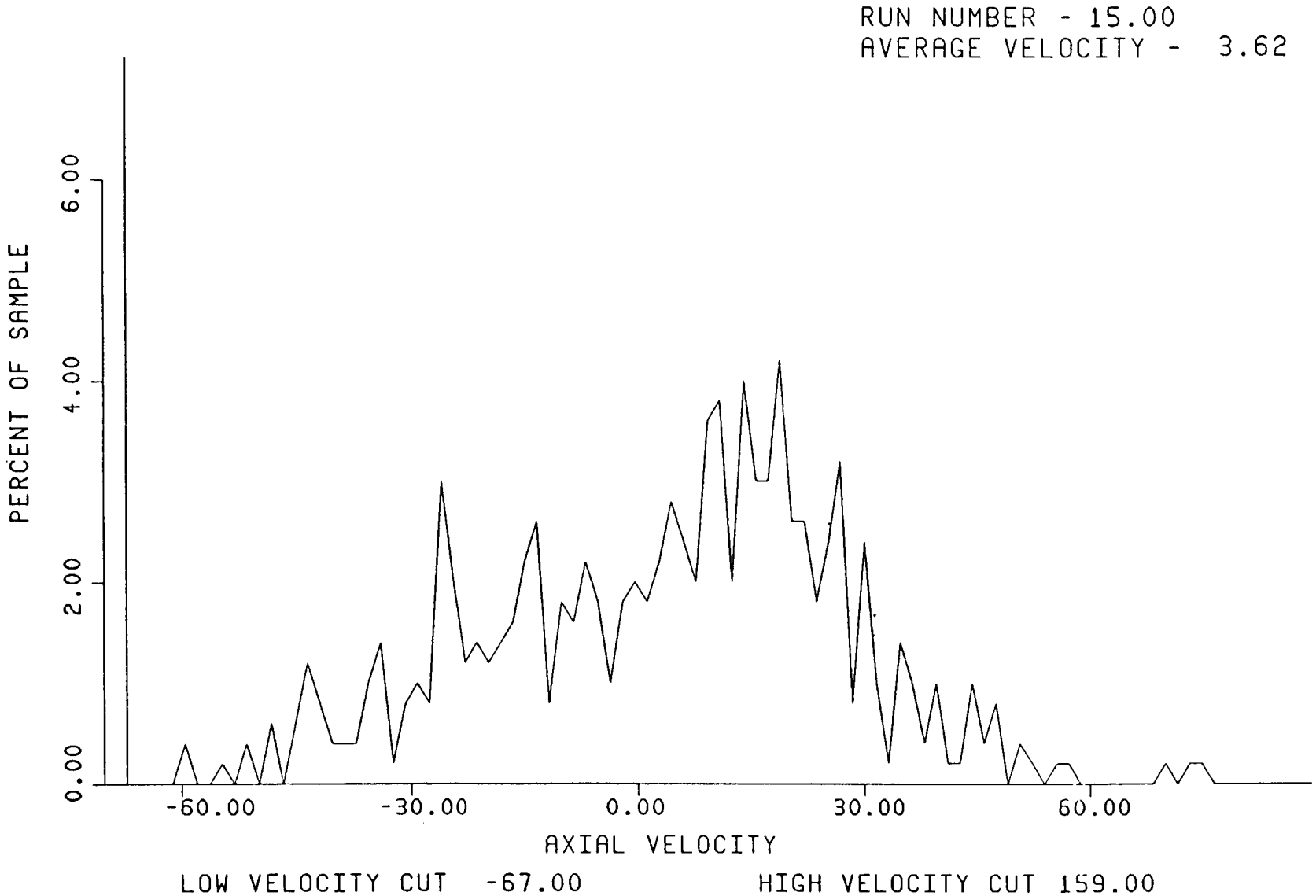

Figure 13. Velocity Probability Histogram for V_∞/V_j = 0.2 h/D_j = 4.0 x/D_j = 1.217 and y/D_j = 0.388

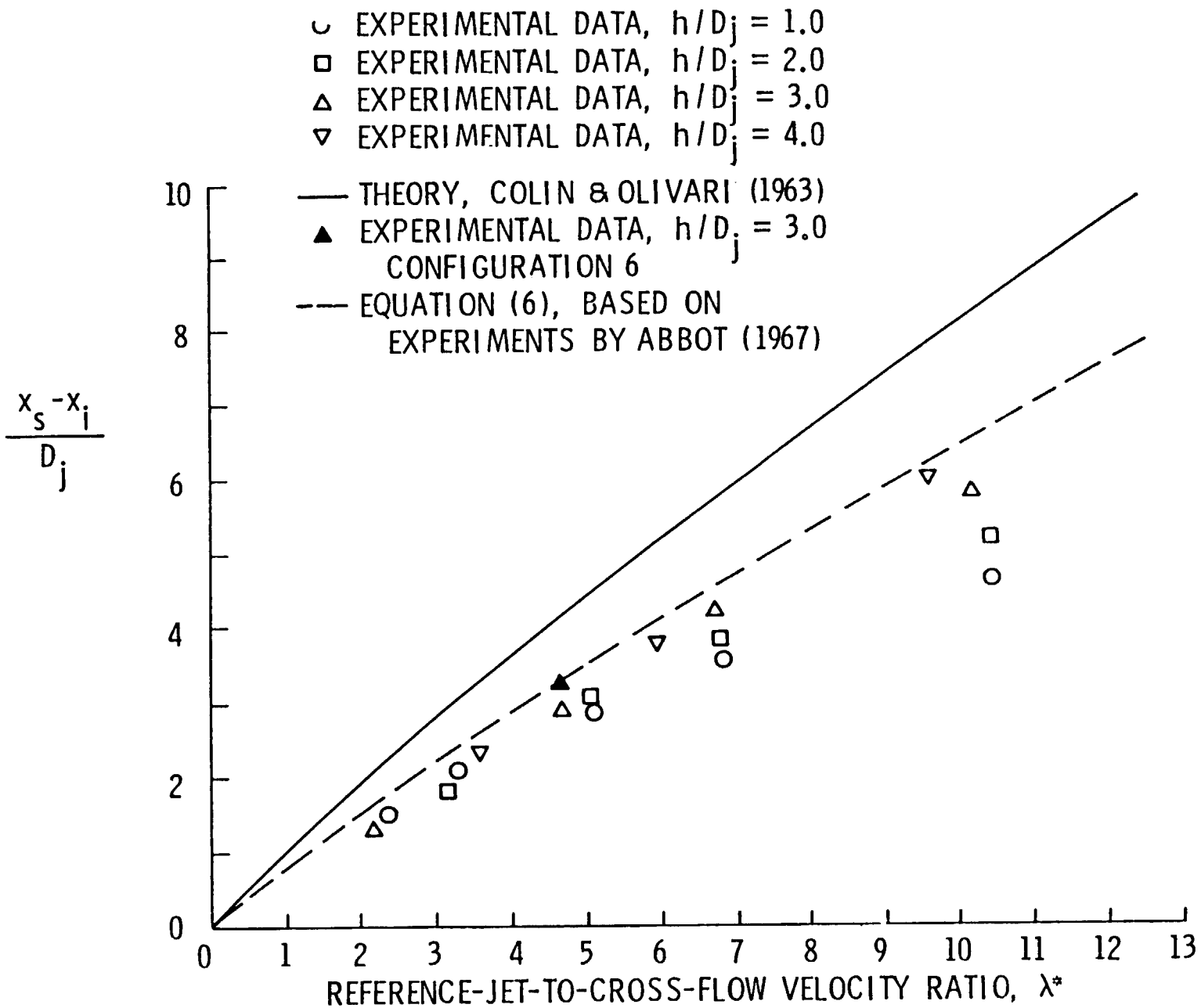

Figure 14. Comparison of Experimental and Theoretical Locations of Separation Points x_s for Various Values of h/D_j